J. Fluid Mech. (2008), *vol.* 607, *pp.* 289–312.
doi:10.1017/S0022112008002097 Printed in the United Kingdom

Miscible porous media displacements driven by non-vertical injection wells

E. UPCHURCH[1] AND E. MEIBURG[2]†

[1]Chevron International Exploration & Production, PO Box 5905, Belair, TX 77402-5095, USA

[2]Department of Mechanical Engineering, University of California, Santa Barbara, CA 93106, USA

(Received 24 September 2007 and in revised form 6 April 2008)

High-resolution simulations are employed to identify and analyse the mechanisms dominating miscible porous media displacements generated by inclined injection wells. Compared to vertical injection wells, significant differences are observed that strongly influence breakthrough times and recovery rates. Constant density and viscosity displacements, for which the velocity field is potential in nature, demonstrate the existence of pronounced flow non-uniformities, due to the interaction of the inclined well with the reservoir boundaries. These non-uniformities deform the fronts during the initial displacement stages.

In the presence of a viscosity difference, the non-uniformities of the potential flow field result in a focusing of the fingering instability. If the fluids also have different densities, a gravity tongue will reinforce the dominant finger along one front, while a gravitational instability leads to the disintegration of the dominant finger along the other front. Hence, the two fronts emerging from the inclined injection well usually evolve very differently from each other for variable density and viscosity displacements.

For inclined injection wells and sufficiently large mobility ratios, gravity tongues are seen to evolve dendritically for an intermediate range of density contrasts. While mild gravitational forces are necessary to create the gravity tongue in the first place, large density differences will suppress the growth of the dendritic side branches. Since the dendritic branches appear along the side of the gravity tongue that should be stable according to traditional stability criteria, it can be concluded that the tip region plays a crucial role in their formation.

1. Introduction

Miscible flooding refers to a process frequently employed in the petroleum industry, in which a miscible solvent injected into oil-bearing rock formations displaces the oil towards the production well. In some variations of this technique, the injection is accomplished by combining vertical wellbores and hydraulically induced fractures: see figure 1 (Bilhartz *et al.* 1978). Such fractures can extend several hundred feet away from the wellbore and are usually vertically oriented. Hence they allow the injection of the miscible solvent in a vertical, plane source configuration, rather than in the more traditional line source configuration.

† Author to whom correspondence should be addressed.

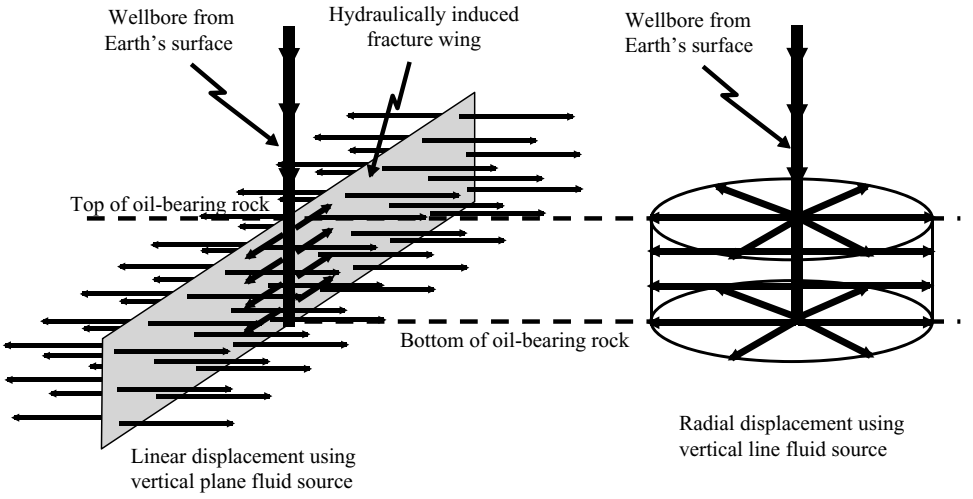

FIGURE 1. A linear displacement using hydraulically induced fractures to create a vertical plane source (*a*), and a simpler radial displacement using a vertical line source (*b*).

The vertical hydraulic fractures are created by injecting a viscous, sand-laden slurry into a rock formation at rates that are much higher than matrix flow in the porous medium can accommodate. Thus, the rock fails and a fracture propagates. If the fluid pressure of the porous srock formation is unaltered from its original state, the fracture will generally propagate vertically and laterally, forming two 'wings' of near-equal lengths that emanate in opposite directions from the vertical wellbore: see figure 1. Continued injection of the viscous sand-laden slurry further propagates and fills the fracture, until the desired fracture dimensions are attained. The viscous liquid phase of the slurry is designed to rapidly lose most of its viscosity within hours of being injected, so that it easily leaks into the surrounding porous rock. It leaves behind a fracture held open with sand whose permeability is usually at least two orders of magnitude larger than the permeability of the rock formation being fractured. In this fashion, the fracture becomes a conduit by which a miscible injected fluid can be easily transmitted horizontally from the vertical wellbore at the centre of the fracture, thereby creating a planar injection source. More details of this technology are described by Howard & Fast (1970).

Vertical plane source configurations for miscible flooding can increase the oil sweep efficiency relative to radial displacements, by lowering viscous fingering and reducing the stranded oil pockets that are common to most radial flooding patterns (Taber & Seright 1992). However, in older oil fields, where the *in situ* fluid pressures of oil-bearing rock formations have been altered from their original state, hydraulically induced fractures have a greater chance of not being vertical. Orientations of up to 49° from the vertical direction have been documented (Wright & Conant 1995). Considering that miscible floods via hydraulic fractures are usually implemented in older oil fields where the pressure regimes have been altered, the occurrence of non-vertical orientations is of great concern. This provides the motivation for the present investigation, which aims to explore the influence of such a non-vertical orientation on miscible displacement processes.

The last half-century has seen enormous progress in our understanding of porous media displacements and the instabilities to which they give rise. Following the early seminal investigations by Hill (1952), Saffman & Taylor (1958), and Chouke,

VanMeurs & Vander Poel (1959), further experimental and theoretical research has provided additional insight on many aspects of such flows, as summarized in the reviews by Homsy (1987) and Yortsos (1990). Linear stability analyses of rectilinear and radial miscible displacements dominated by diffusion and/or dispersion were put on sound theoretical footing by the work of Tan & Homsy (1986), Hickernell & Yortsos (1986), Tan & Homsy (1987), Yortsos & Zeybek (1988) and Riaz & Meiburg (2003*a*). Subsequent work addressed the influence on the interfacial stability of such features as tangential velocity difference across the interface (Rogerson & Meiburg 1993*a*), non-monotonic viscosity profiles (Manickam & Homsy 1993), variable density effects (Manickam & Homsy 1995) and concentration-dependent diffusion (Riaz & Meiburg 2004). In spite of the early work by Peaceman & Rachford (1962), high-resolution nonlinear simulations began to have a stronger impact on the field only more recently. The investigations by Tan & Homsy (1988), Christie (1989), Zimmerman & Homsy (1992*b*), Rogerson & Meiburg (1993*b*), Manickam & Homsy (1994), Tchelepi (1994), Chen & Meiburg (1998*a*), Pankiewitz & Meiburg (1999), De Wit & Homsy (1999), Ruith & Meiburg (2000) and Riaz & Meiburg (2003*b*) explore various aspects of two- and three-dimensional miscible displacements, based on the assumption of homogeneous permeability and isotropic dispersion. Heterogeneous displacements are addressed by Tan & Homsy (1992), Chen & Meiburg (1998*b*), Camhi, Meiburg & Ruith (2000) and Riaz, Pankiewitz & Meiburg (2004), whereas Zimmerman & Homsy (1991, 1992*a*), Tchelepi (1994) and Yang & Yortsos (1998) focus on the influence of anisotropic dispersion.

In all of the above studies, planar or line injection sources are assumed that are oriented orthogonally to the main flow direction. Hence they do not provide information on the central question under consideration here, which concerns the influence of inclined injection wells. Section 2 sets up the model problem that will be studied in order to address this issue. The governing equations, boundary and initial conditions will be stated, and the computational approach will be outlined briefly. Subsequently, § 3 will describe the nature of the potential flow field, which is due to the reservoir geometry and the injection configuration alone, and which governs the simplified problem of a constant density and viscosity displacement. Understanding the features of this potential flow subsequently will be crucial for analysing the mechanisms that dominate variable density and viscosity displacements, as described in § 4. Section 5 summarizes the findings from this investigation and discusses the main conclusions to be drawn.

2. Problem formulation

In order to investigate miscible porous media displacements generated by inclined injection wells, we focus on the two-dimensional model configuration of a horizontal reservoir of height H, length W, and aspect ratio $A = H/W$: see figure 2. An injection well located at the centre, and inclined by an angle α with regard to the vertical, injects a constant rate Q of fluid volume per unit spanwise width, equally distributed along its length. The injected fluid of density ρ_1 and viscosity μ_1 is miscible in all proportions with the resident fluid of ρ_2 and μ_2, subject to a constant diffusion coefficient D. The variable c indicates the local volume concentration of the injected fluid. The upper and lower boundaries of the reservoir are impenetrable, while vertical production wells are placed at the left and right reservoir boundaries. We aim to investigate the temporal evolution of the front separating the injected and the displaced fluid, from

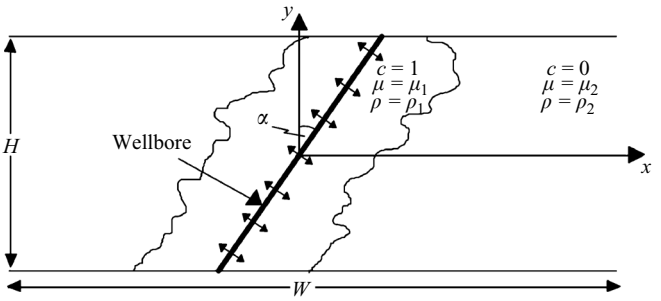

FIGURE 2. Schematic of the miscible flow due to an inclined planar injection source. The resident fluid 2, characterized by viscosity μ_2 and density ρ_2, is displaced by the injected fluid 1, with μ_1 and ρ_1. The horizontal rectangular reservoir is of height H and width W, and it has a constant permeability k. The injection source is inclined by an angle α with regard to the vertical direction.

the start of the injection up to the time when the displacement front first reaches one of the production wells.

2.1. *Governing equations*

We assume the reservoir permeability k to be constant and isotropic, so that the permeability is identical in the horizontal and vertical directions. Under these conditions, Darcy's law takes the form

$$\nabla p = -\frac{\mu}{k}\boldsymbol{u} - \rho g \nabla y, \tag{2.1}$$

where p represents pressure, $\boldsymbol{u}$ is the fluid velocity, and g indicates the gravitational acceleration. The concentration field c of the displacing fluid is governed by a convection–diffusion equation of the form

$$\frac{\partial c}{\partial t} + \boldsymbol{u}\cdot\nabla c = (1-c)\,\nabla\cdot\boldsymbol{u} + D\nabla^2 c, \tag{2.2}$$

where

$$\nabla\cdot\boldsymbol{u} = q \tag{2.3}$$

denotes the local source strength of the injected fluid (Chen & Meiburg 1998*a*).

A few comments are in order regarding the assumption of a constant and isotropic diffusion coefficient D between the injected and displaced fluids in (2.2). Frequently, at the slow displacement velocities found in petroleum reservoirs, molecular diffusion dominates over flow-induced dispersion, as first indicated by Blackwell, Rayne & Terry (1959) and later confirmed by van der Poel (1962), Perkins & Johnston (1963) and Stalkup (1983). On the other hand, the higher fluid velocities commonly employed in laboratory experiments result in velocity-dependent, anisotropic dispersion (Taylor 1953) to dominate, as described by Perkins & Johnston (1963), Gardner & Ypma (1984), Christie & Bond (1986), Christie (1989), Coskuner & Bentsen (1990), Christie, Jones & Muggeridge (1990), Bacri, Salin & Woumeni (1991), Bacri *et al.* (1992), Zimmerman & Homsy (1992*b*), Tchelepi (1994), Petitjeans & Maxworthy (1996), Chen & Meiburg (1996) and Petitjeans *et al.* (1999), among others. A more detailed discussion of this topic is provided by Upchurch (2005).

We non-dimensionalize (2.1)–(2.3) by scaling all lengths with H, time with H^2/Q, and velocity with Q/H. Note that this approach differs from the diffusion-based scaling employed by other authors (e.g. Tan & Homsy 1986; Rogerson & Meiburg

1993*a*; Tchelepi 1994; Manickam & Homsy 1995) for problems without an externally imposed length scale. The variables p, ρ, μ and c are rendered dimensionless by using $\mu_1 Q/k$, $\Delta\rho = \rho_2 - \rho_1$, μ_1 and c_1, respectively. As dimensionless forms of (2.1)–(2.3) we thus obtain

$$\nabla \cdot \boldsymbol{u} = q, \tag{2.4}$$

$$\frac{\partial p}{\partial x} = -\mu u, \tag{2.5}$$

$$\frac{\partial p}{\partial y} = -\mu v - G\rho, \tag{2.6}$$

$$\frac{\partial c}{\partial t} + \boldsymbol{u} \cdot \nabla c = (1-c)\,\nabla \cdot \boldsymbol{u} + \frac{1}{Pe}\nabla^2 c. \tag{2.7}$$

Here the gravity parameter

$$G = \frac{(\rho_2 - \rho_1)\,Hgk}{\mu_1 Q} \tag{2.8}$$

represents the ratio of gravitational to viscous forces, while the Péclet number

$$Pe = \frac{Q}{D} \tag{2.9}$$

indicates the relative importance of convective and diffusive transport on the concentration field.

It remains to specify the variation of density and viscosity with the injected fluid concentration. Here we follow earlier authors (e.g. Tan & Homsy 1986) and employ

$$\rho(c) = \frac{\rho_2}{(\rho_2 - \rho_1)} - c \tag{2.10}$$

along with

$$\mu(c) = \mathrm{e}^{R(1-c)}, \quad R = \ln\left(\frac{\mu_2}{\mu_1}\right). \tag{2.11}$$

By cross-differentiating (2.5) and (2.6) to eliminate pressure, and defining the vorticity ω according to

$$\omega = \frac{\partial v}{\partial x} - \frac{\partial u}{\partial y}, \tag{2.12}$$

we obtain

$$\omega = -R\left(u\frac{\partial c}{\partial y} - v\frac{\partial c}{\partial x}\right) + \frac{G}{\mu}\frac{\partial c}{\partial x}. \tag{2.13}$$

The above form of the vorticity equation is equivalent to the one first shown by Heller (1963); see also De Josselin De Jong (1960). It indicates that vorticity is present in the flow field at locations where density and viscosity vary, as a result of local concentration gradients. Consequently, the vorticity variable provides a well-suited tool for analysing the effects of viscosity and density variations, and their mutual interactions, onto the overall displacement flow. Hence we follow other authors (Tryggvason & Aref 1983; Meiburg & Homsy 1988; Tan & Homsy 1988; Chen & Meiburg 1998*a*; Ruith & Meiburg 2000; and others), and decompose the velocity field into a potential component $\boldsymbol{u}_{pot}$ that reflects the presence of the injection well and the boundaries, and a rotational component $\boldsymbol{u}_{rot}$ that captures the effects of viscosity and density variations

$$\boldsymbol{u} = \boldsymbol{u}_{pot} + \boldsymbol{u}_{rot}. \tag{2.14}$$

Finally, we introduce the streamfunction ψ according to

$$u = \frac{\partial \psi}{\partial y}, \quad v = -\frac{\partial \psi}{\partial x}. \tag{2.15}$$

Our system of governing dimensionless equations thus takes the form

$$\nabla^2 \psi = -\omega, \tag{2.16}$$

$$\omega = -R \nabla \psi \cdot \nabla c + \frac{G}{\mu} \frac{\partial c}{\partial x}, \tag{2.17}$$

along with (2.7) for the concentration field. As boundary conditions for the streamfunction and concentration fields, we have

$$x = \pm \frac{0.5}{A} : \ \frac{\partial \psi}{\partial x} = 0, \quad \frac{\partial c}{\partial x} = 0, \tag{2.18}$$

$$y = \pm 0.5 : \ \psi = 0, \quad \frac{\partial c}{\partial y} = 0. \tag{2.19}$$

Note that the above conditions effectively impose symmetry at the left and right boundaries.

Ideally, we would impose the initial condition of potential flow everywhere, along with $c = 1$ at the source location and $c = 0$ elsewhere. Physically, such a discontinuous initial condition for the concentration field would be smoothed in time by diffusion. Computationally, however, the initial discontinuity can trigger unphysical oscillations, and hence numerical instability. Hence, we spread out the initial concentration front over a small distance on each side of the source by means of an error function distribution, in order to obtain a smooth initial concentration field. For details, the reader is referred to Upchurch (2005).

2.2. *Computational approach*

The simulations typically employ a computational domain of aspect ratio $A = 1/10$, which is discretized into 2048×200 grid points. Test simulations found this discretization to be sufficient for the range of Péclet numbers, mobility ratios and gravity parameters employed in the present investigation. In particular, this discretization ensures that numerical diffusion is always significantly smaller than physical diffusion. The concentration equation is stepped forward in time by means of a second-order-accurate alternating direction implicit (ADI) technique (Peaceman & Rachford 1955), where the fluid velocities in the nonlinear term are taken at the old time level. The Poisson equation for the rotational component of the streamfunction is solved by a spectral approach (Canuto *et al.* 1988) in the x direction, combined with 6th-order compact finite differences (Lele 1992) in the y direction.

2.2.1. *Representation of the potential flow field*

The inclined line source is discretized into N point sources of equal strength, as sketched in figure 3. The horizontal boundaries at the top and bottom of the computational domain are accounted for by an infinite (in the y direction) series of mirror images of these sources, based on the closed-form expressions provided by Lamb (1932). In order to avoid singularities in the flow field, the point sources within the computational domain, as well as their extensions immediately above and below, are smoothed according to a Gaussian distribution of radius ξ, as described in detail in Upchurch (2005). Typically, we chose $N = 200$ and $\xi = 0.005$. These parameters were selected such that a further increase in N did not result in a noticeable change

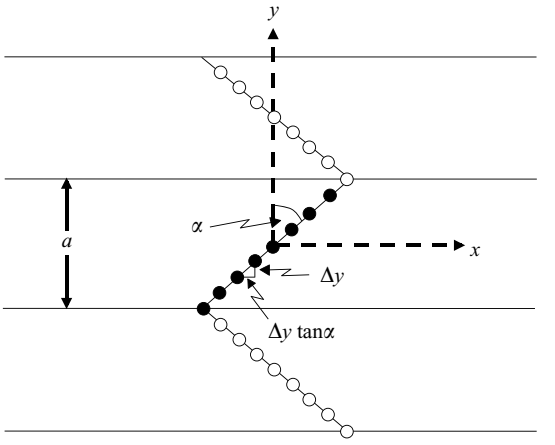

FIGURE 3. Schematic showing the use of smoothed point sources to represent the inclined injection well. The method of images is employed to account for the top and bottom reservoir boundaries.

of the flow field. Note that for these parameters there exists substantial overlap of the smoothed point sources, so that the non-uniformity of the injection well is minimized. Furthermore, at the start of the simulation the error-function-like fronts are located beyond the radius of these smoothed point sources, so that the remaining non-uniformities do not affect the fronts.

2.3. *Validation*

The simulation procedure was validated by comparing both early and late time results for vertical injection wells to published data. For early times, unstable viscosity ratios $R > 0$ and $G = 0$, the preferred wavenumber of emerging fingers for a vertical injection well was compared with linear stability results of Tan & Homsy (1986), which are based on the quasi-steady-state assumption. Good quantitative agreement was obtained: see figure 4. For late times, we compared long-term simulation results for vertical injection wells, $R > 0$ and $G > 0$, with corresponding data obtained by Tchelepi (1994). Close qualitative and quantitative agreement was observed for both the growth of the mixing region and the number of well-developed fingers. More details can be found in Upchurch (2005).

3. Characteristics of the potential flow field

A vertical source ($\alpha = 0°$) yields purely horizontal streamlines and a constant velocity magnitude of one half, except for right at the injection source, where the velocity decreases to zero due to the smoothing of the point sources. Placing the injection source at an inclined angle will deform the streamlines, due to the interaction of the source with the impenetrable top and bottom reservoir boundaries. Near the line source, the streamlines will be oriented perpendicularly to the source. On the other hand, the presence of the reservoir boundaries enforces a horizontal streamline direction in the far field. Consequently, the potential velocity field develops a degree of non-uniformity that increases with the inclination angle α. Example streamline patterns are shown in figure 5 for $\alpha = 30°$, 45° and 60°. Note that along the central section of the line source the streamlines maintain a direction approximately

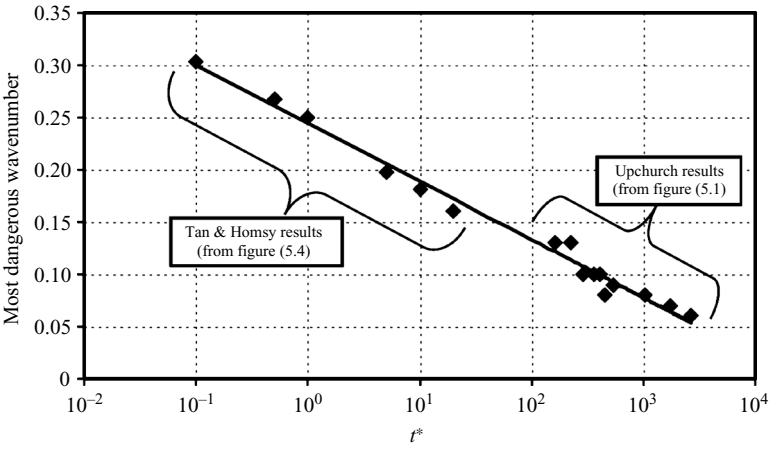

FIGURE 4. Comparison of the preferred early-time wavenumbers obtained in the present, nonlinear simulations, with the linear stability results of Tan & Homsy (1986), for $R = 3$, after Upchurch (2005). Good quantitative agreement is obtained. Following those authors, time in this figure is rendered dimensionless via diffusive scaling.

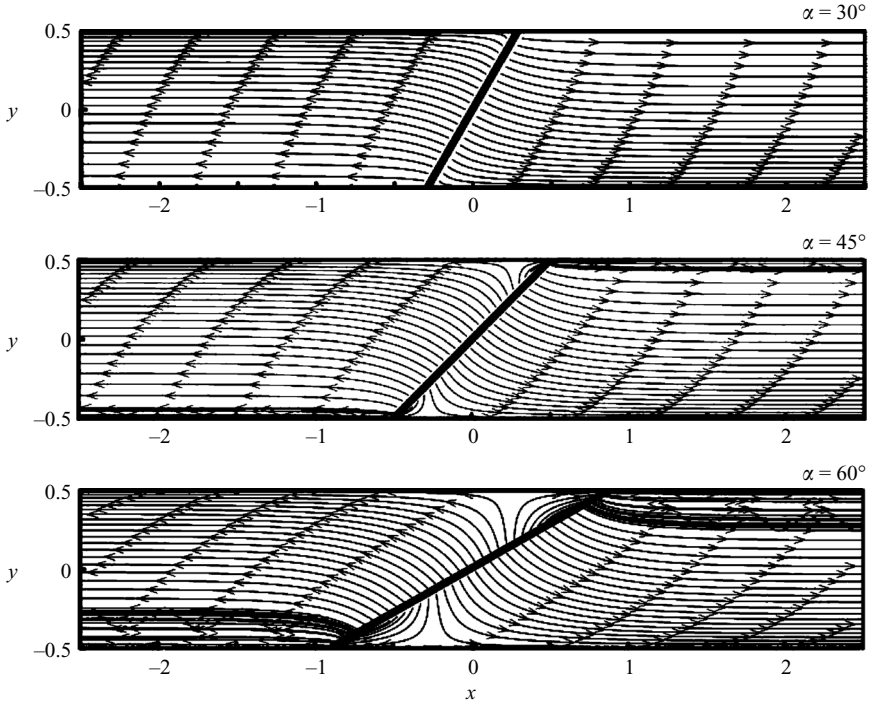

FIGURE 5. Potential flow streamlines for $\alpha = 30°$, 45° and 60°. The streamlines were generated by tracing the velocity field, starting from equally spaced locations along the line source. The inclination of the line source, in combination with the impenetrable top and bottom reservoir boundaries, causes the potential velocity field to be non-uniform near the injection well. For large inclination angles, a stagnation point is seen to emerge where the line source forms an acute angle with the boundary.

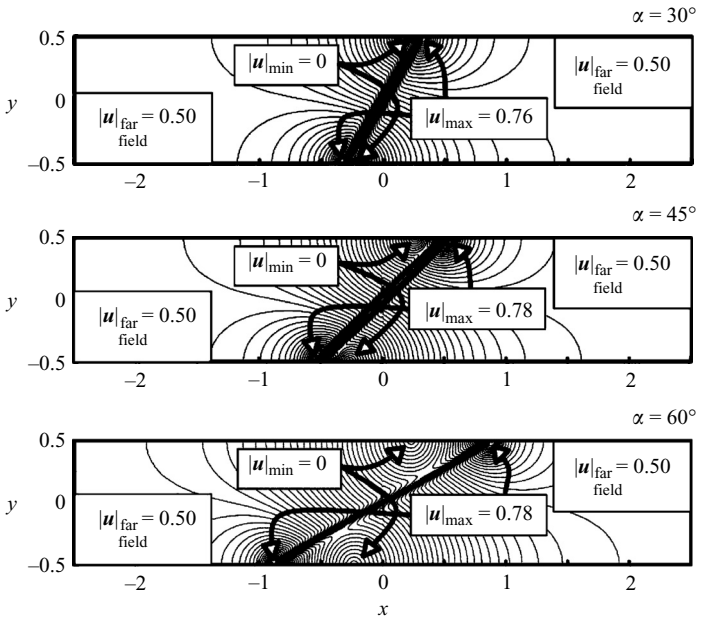

FIGURE 6. Velocity magnitude contours for $\alpha = 30°$, 45° and 60°, respectively. The contour interval is 0.015. In the vicinity of the acute angle, near the stagnation point, an area of slow flow exists, while the region of the obtuse angle shows accelerated flow.

perpendicular to the source. However, the presence of reservoir boundaries causes the emergence of a stagnation point where the source forms an acute angle with the boundary. As α increases, this stagnation point moves farther away from the intersection of the well with the reservoir boundary. It causes some of the injected fluid to turn around and to flow across the injection well. Hence the local volume flux increases on the other side of the well, where it forms an obtuse angle with the boundary.

A detailed evaluation shows that the velocity maximum found in this region remains fairly constant at about $0.76 \leqslant |u_{\max}| \leqslant 0.78$ for angles in the range $30° \leqslant \alpha \leqslant 60°$: see figure 6. Far away from the injection well, the velocity field approaches a uniform parallel flow with constant velocity for all cases. We can estimate the region of non-uniformity to extend over a distance of $O(\tan\alpha)$ away from the centre of the domain.

The non-uniform potential flow velocity field distinguishes the present displacement from earlier, rectilinear displacements in which the well was oriented perpendicularly to the main flow direction, e.g. Tan & Homsy (1988) and Ruith & Meiburg (2000). This non-uniform flow is expected to affect the displacement front in multiple ways. Firstly, even if the front were convected as a passive scalar, it would be stretched and tilted as a result of local potential velocity gradients. Secondly, for unfavourable mobility ratios the variations in the potential velocity field will result in uneven fingering along the front. In regions of high velocities normal to the front, viscous fingering will be amplified, so that we expect to observe more and stronger fingers. On the other hand, in regions of smaller fluid velocity fingering activity should decrease. Finally, for variable density displacements the stretching and tilting of the interface by the non-uniform potential velocity field can be expected to create local regions of unstable density stratification, in which gravitational fingering may occur. The goal

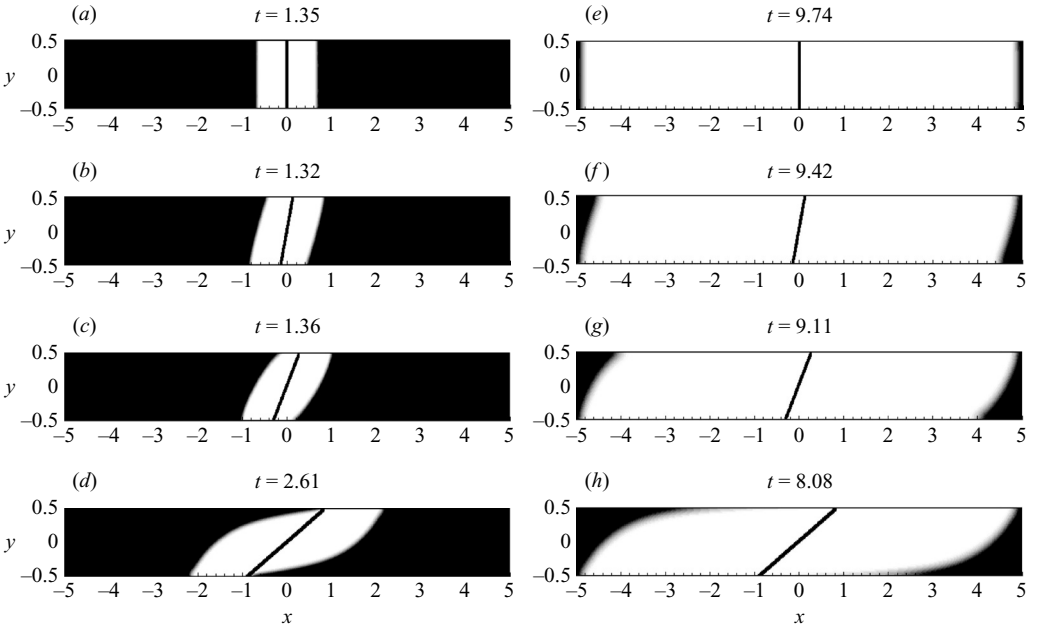

FIGURE 7. Early (*a*)–(*d*) and late (*e*)–(*h*) time displacement front configurations for $R = G = 0$, $Pe = 2000$ and source inclination angles of $\alpha = 0°$, 15°, 30° and 60°, respectively. For these constant density and viscosity displacements, the concentration field is passively convected by the potential velocity field. During the early stages, the fronts are deformed as a result of the non-uniformity of the potential velocity fields in the vicinity of the injection wells. Later on, they are being convected in the nearly uniform velocity far field, without significant further deformation.

of the present investigation is to explore how these scenarios play out quantitatively, and how they are coupled to secondary, vortical flow patterns.

4. Results

4.1. *Negligible viscosity difference,* $R = 0$

4.1.1. *Constant density displacements,* $G = 0$

Constant viscosity and density displacements allow us to examine how the potential flow field influences the miscible flood front. Under these conditions, the front is convected by the potential flow field as a passive, diffusing scalar. Figure 7 displays representative displacement fronts for various source inclinations α, at both early and late times. As the source angle increases, the distortion of the front during the early stages of the displacement becomes more pronounced, in accordance with the growing spatial non-uniformities of the potential flow field. In particular, the acceleration and deceleration of the front near the velocity maximum and the stagnation point, respectively, can be recognized. Note that the stretching and tilting of the front takes place during the early stages only, when the front migrates through the non-uniform regions of the potential flow field in the vicinity of the injection source. For these early stages of the displacement, the local velocity of the front depends strongly on the inclination angle. Since the non-uniformity of the potential velocity field extends a distance of $O(\tan\alpha)$ away from the centre of the domain, and the front moves with $O(1)$ maximum horizontal velocity, the early stages last for $O(\tan\alpha)$ dimensionless

time units. During the later stages, the front finds itself in regions of nearly uniform, parallel potential flow, and its velocity asymptotically reaches a value of one half. Any deformation during this phase is due to a combination of molecular diffusion and flow-induced dispersion (Taylor 1953; Petitjeans & Maxworthy 1996; Chen & Meiburg 1996; Petitjeans *et al.* 1999).

As the source inclination angle increases, the stagnation points located at the horizontal reservoir boundaries move away from the intersection of these boundaries with the line source. As discussed above, this causes a fraction of the injected fluid to turn back towards the source. Hence, the section of the front that crosses the stagnation point streamline undergoes continued stretching. In the absence of diffusion, this stretching would persist for all times, and the stretched interface would reach the top and bottom reservoir boundaries only asymptotically. For the present miscible case, however, diffusion causes the injected fluid to spread to these boundaries after a time that depends on Pe.

4.1.2. *Variable density displacements,* $G > 0$

Equation (2.17) states that variable density displacements result in the production of vorticity along the interface, due to the presence of horizontal concentration gradients. For constant permeability and viscosity, the dimensional vorticity field is given by

$$\omega = -\frac{gk}{\mu}\rho_x. \tag{4.1}$$

By integrating across the finite-width interface, we can determine the circulation-per-unit interface length as

$$|\gamma| = \frac{gk}{\mu}\,\Delta\rho\,\cos\theta, \tag{4.2}$$

where θ is the local angle of inclination of the interface with respect to the vertical direction. The overall circulation associated with each front between the top and bottom reservoir boundaries then is

$$|\Gamma| = \frac{gk\,\Delta\rho\,H}{\mu}. \tag{4.3}$$

As shown in figure 8 for a set of representative angles and $G = 0.5$, this circulation destroys the point symmetry of the flow with regard to the centre of the domain. It rotates the displacement fronts in such a way that the lighter fluid moves above the denser one, i.e. into a gravitationally stable position; see also the earlier observations by Christie *et al.* (1990), Tchelepi (1994) and Ruith & Meiburg (2000). For the purpose of determining a characteristic time scale associated with the interface rotation, let us assume that all of the circulation associated with a front is concentrated in a point vortex at the centre of the front ($y = 0$). The angular velocity induced by this point vortex at the upper and lower reservoir boundaries provides a characteristic time scale for the interface rotation in the form of

$$t_{rot} = \frac{H\mu}{gk\,\Delta\rho}. \tag{4.4}$$

The early frontal shape is governed by the interaction of gravitational rotation and the deformation due to the non-uniform potential flow. For the right-propagating fronts in figure 8, both of these effects tend to rotate the front in the clockwise direction. For the left-propagating fronts, the non-uniformity due to the injection well tilts the front in the clockwise direction, while gravity causes a rotation in the opposite direction.

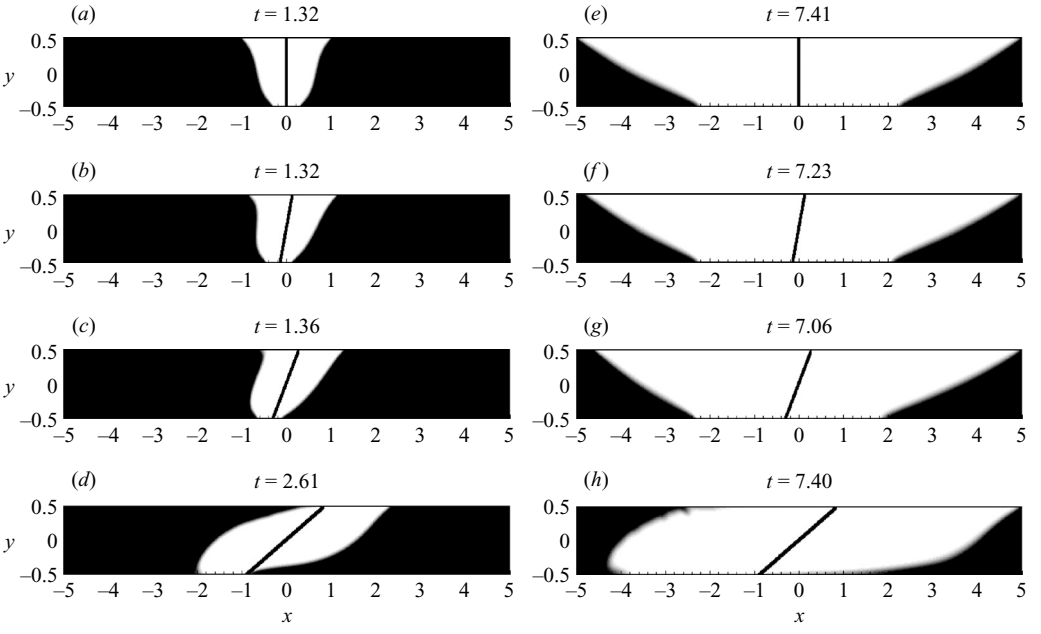

FIGURE 8. Early (*a*)–(*d*) and late (*e*)–(*h*) time displacement front for $R = 0$, $G = 0.5$, $Pe = 2000$ and source inclination angles of $\alpha = 0°$, 15°, 30° and 60°, respectively. The density difference results in the gravitational rotation of the interfaces, thereby breaking the symmetry of the flow. For $\alpha \leqslant 30°$, the left front is tilted rapidly enough to suppress gravitational fingering. For $\alpha = 60°$, notice the incipient fingering in the upper section of the left interface at late times.

The figure demonstrates that for early times the source effect dominates. During the later stages, however, the front has moved away from the source, so that the influence of the non-uniformity declines, whereas gravity maintains its action. Hence, during the later flow stages in figure 8 the left frontal shapes are dominated by gravity for all but the largest source inclination angle. With regard to the overall propagation velocity of the left front, the opposing influences of the non-uniformity and gravity partially cancel each other. Hence the left front propagates more slowly than the right one, which reaches the vertical boundary of the domain ('breaks through') first.

An interesting question concerns the long-term evolution of the left-propagating front in figure 8(*d*, *h*). As one possibility, the continued action of gravity might cause the front to rotate into a gravitationally stable configuration, until it resembles the frontal shapes of figures 8(*a*–*c*) and 8(*e*–*g*). Alternatively, we note that in figure 8(*d*, *h*) denser (black) fluid is situated above less dense (white) fluid, so that the possibility of a gravitational instability at the interface arises. In fact, close inspection of figure 8(*d*, *h*) indicates the presence of small undulations along the top section of the left-propagating front at late times, which reflect the incipient stages of such an instability.

As G increases to 1, this instability becomes clearly visible already during the earlier stages (see figure 9), and significant gravity-driven fingering can be observed. This fingering process encapsulates pockets of the more viscous fluid behind the front, which gradually diffuse into the surrounding injected fluid. For long times, the frontal tilting by gravity results in lighter fluid being placed above heavier fluid, so that any fingering activity ceases.

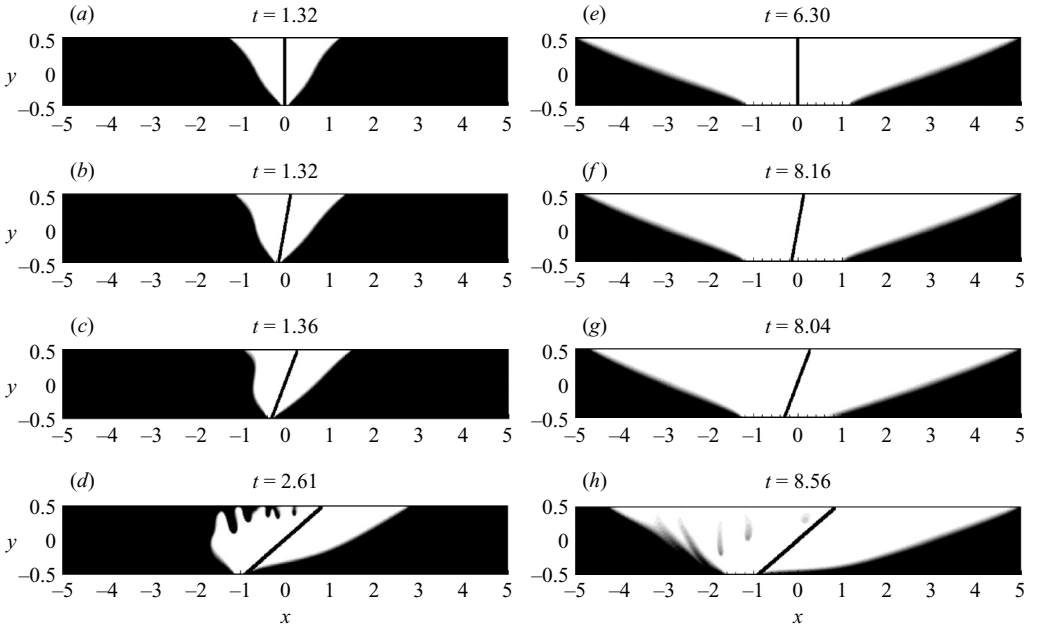

FIGURE 9. Displacement fronts for $R = 0$, $G = 1$, $Pe = 2000$ and source inclination angles of $\alpha = 0°$, 15°, 30° and 60°, respectively. For this larger value of G, the tilting of the left front proceeds more rapidly. However, for the largest source inclination angle gravitational fingering sets in before the front has been rotated sufficiently far to suppress the gravitational instability.

Analysing the gravitationally unstable situation of a denser fluid placed above a lighter one along a quiescent front, Manickam & Homsy (1995) identify the characteristic time scale for the growth of gravitational fingers as

$$t_{grav} = \frac{D\mu^2}{g^2 k^2 \, \Delta\rho^2}. \tag{4.5}$$

Hence, for gravitational fingers to grow before the left interface has been rotated sufficiently to suppress such fingering, the ratio

$$\frac{t_{rot}}{t_{grav}} = Pe\, G \tag{4.6}$$

has to be sufficiently large. The required value of $Pe\, G$ for gravitational fingering to occur depends on the source angle, as the interface has to be rotated further for large α in order to suppress gravitational fingering. The comparison of figures 8 and 9 is consistent with the scaling law (4.6), in that it shows gravitational fingering becoming more prominent for increasing G, even though the interface is rotated into a stable position more rapidly.

In summary, even for the relatively simple situation of a constant viscosity displacement, we identify three time scales associated with (i) the propagation of the front through the non-uniform part of the potential velocity field near the injection well, (ii) the rotation of the front due to gravitational vorticity, and (iii) the gravitational fingering instability. The relative magnitude of these three time scales determines the evolution of the flow.

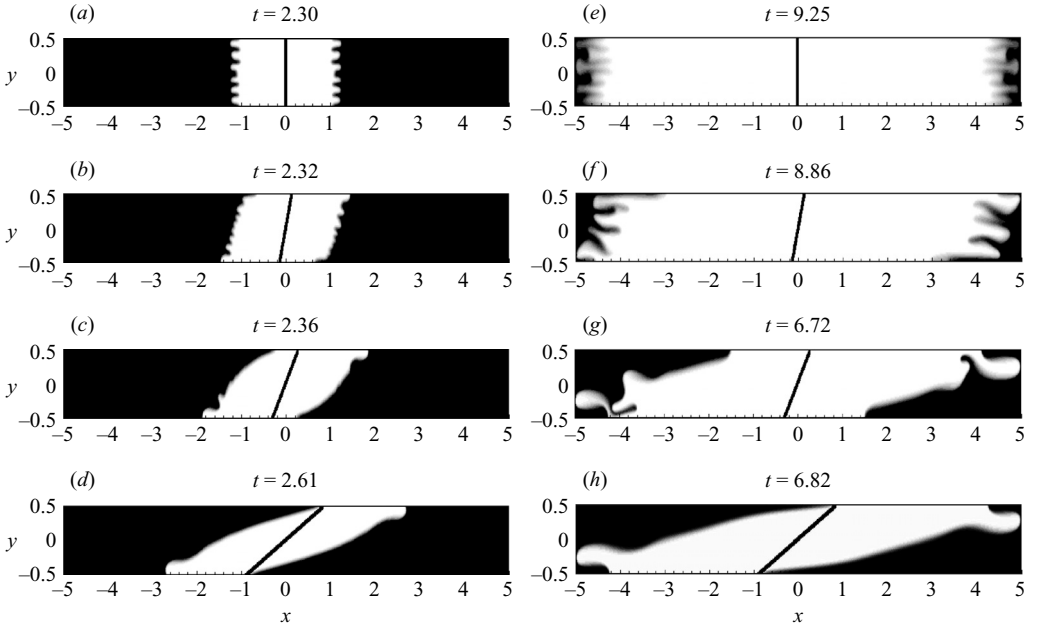

FIGURE 10. Displacement fronts for $R = 1$, $G = 0$, $Pe = 2000$ and source inclination angles of $\alpha = 0°$, 15°, 30° and 60°, respectively. As the angle of inclination grows, the uniform viscous fingering pattern gives way to configurations dominated by a single finger propagating along the reservoir boundary. This reflects a focusing of the viscous fingering instability by the velocity maximum in the non-uniform potential flow field.

4.2. *Moderate viscosity difference,* $R = 1$

4.2.1. *Constant density displacements,* $G = 0$

Even a moderate amount of unfavourable viscosity difference results in the growth of fingers for the case of a vertical injection well: see figure 10 (a, e). Here the fingering pattern is rather homogeneous, as the potential velocity field is spatially uniform.

For a source inclination angle of $\alpha = 15°$, the spatial variations in the potential velocity field begin to modify the fingering pattern. Fingers grow more rapidly in the region of the obtuse angle between the source and reservoir boundary, where the potential flow is accelerated. Conversely, their growth is damped in the vicinity of the stagnation points where the source and the reservoir boundary form an acute angle. This observation is consistent with the basic stability criterion for viscous fingering (Saffman & Taylor 1958; chouke *et al.* 1959), which states that the destabilizing influence is proportional to the product of the viscosity difference and the velocity component normal to the interface. However, this influence of the potential flow field non-uniformity is limited to early times. During the later stages the fronts move through a nearly uniform, parallel potential flow, so that the fingering pattern becomes more uniform. Consequently, near the time of breakthrough the fingering patterns for $\alpha = 0°$ and 15° are quite similar.

Larger angles of inclination give rise to more pronounced differences. For $\alpha = 30°$ and 60°, fingers emerge only in the regions of accelerated potential flow, whereas much of the front does not exhibit any fingering. This stabilization of large sections of the front reflects a combination of three effects, viz. (i) the local reduction in the magnitude of the potential flow velocity, (ii) the large angle of interfacial inclination,

which further reduces the normal component of the potential flow velocity, and (iii) the presence of a tangential velocity difference across the interface, which is known to be stabilizing (Rogerson & Meilburg 1993*a*, *b*). Even for long times, these large-α flows are dominated by single fingers propagating along the top and bottom reservoir boundaries. Note that these fingers are unrelated to the phenomenon of gravity tongues (Ruith & Meiburg 2000), as there is no density contrast in the present flow.

In summary, we find that for unfavourable viscosity differences the inclination of the injection well leads to a 'focusing' of the viscous fingering instability in the region of large-potential flow velocity. This focusing results in the rapid formation of a single dominant finger, which causes the front to break through significantly earlier than for a vertical injection well.

We remark that for the cases shown in figure 10 the governing equations, boundary and initial conditions are symmetric with respect to the centre of the domain. Nevertheless, small asymmetries can be detected in the late-stage flow patterns. These are due to the amplification of random numerical perturbations by the fingering instability. There are several potential sources for introducing such small numerical errors. These sources include the spatial and the time discretization in general (e.g. the direction sequence of the ADI procedure), the use of the Gaussian sources and their images, and others.

4.2.2. *Variable density displacements,* $G > 0$

For unfavourable viscosity ratios and $G > 0$, the displacements are dominated by a competition between the gravity- and viscosity-driven mechanisms that were discussed above in isolation. How this competition plays out depends on the inclination angle, and the potential flow field it generates. Representative early- and late-time displacement fields are shown in figure 11 for $G = 0.5$. The case of a vertical injection well demonstrates the tendency of the flow to form a gravity tongue. Note that this results in the suppression of viscous fingering, which had been prominent in the $G = 0$ counterpart. The explanation for this observation lies in the stabilization of the interface by gravitational forces, which lead to a reduced normal velocity, since the fluid now has a strong upward velocity component, and a tangential velocity difference across the interface (Rogerson & Meiburg 1993*a*); see also Ruith & Meiburg (2000). Note that, in comparison to the constant viscosity case shown in figure 8, the fronts break through earlier, as the growth of the gravity tongue is now amplified by the unfavourable mobility ratio.

For all non-zero angles of inclination, we recognize a clear difference in the evolution of the two fronts. The right-propagating front is stable to fingering in all cases. Here, the tendency of the $R = 0$, $G = 0.5$ flow to form a gravity tongue (figure 8) is reinforced by the tendency of the focusing mechanism observed for the $R = 1$, $G = 0$ case (figure 10) to form a dominant viscous finger along the top boundary. This reinforcement is confirmed by the bottom frame in the right column, which shows the rotational streamlines superimposed on the concentration gradient field. These streamlines indicate a strong clockwise vortex centred around the right-propagating front, which accelerates the top section of this front. As a result, the right-propagating front reaches the end of the computational domain more quickly than the constant viscosity and constant density flows discussed above.

On the other hand, the left-propagating front shows pronounced fingers for all non-vanishing angles of inclination. For $\alpha = 15^\circ$ and early times, the clockwise front rotation by the potential flow field is approximately balanced by the anticlockwise

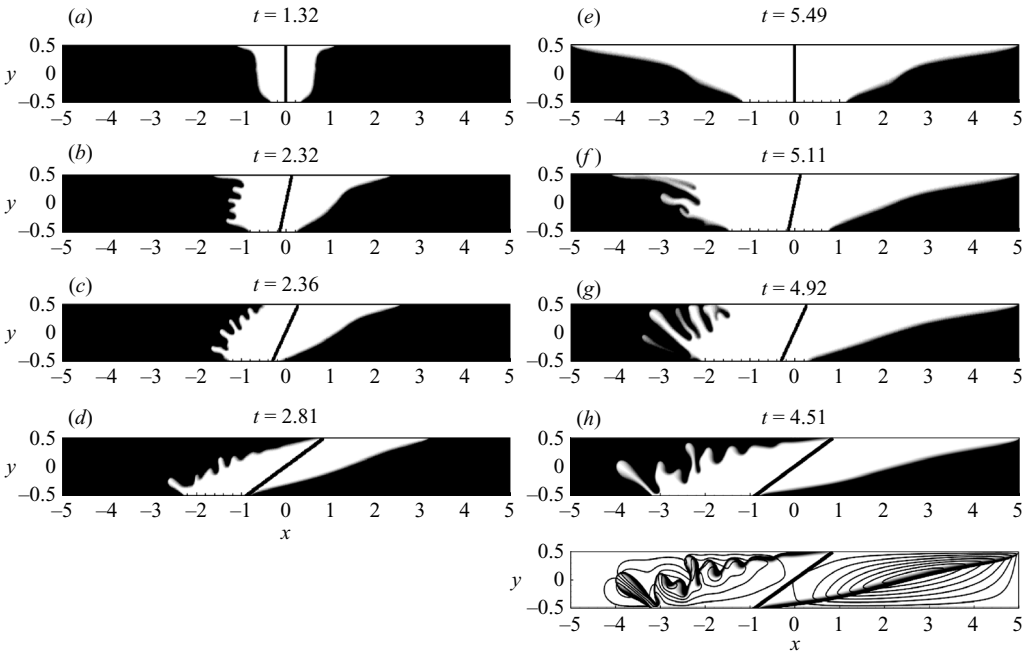

FIGURE 11. Displacement fronts for $R = 1$, $G = 0.5$, $Pe = 2000$ and source inclination angles of $\alpha = 0°$, 15°, 30° and 60°, respectively. For the right-propagating fronts at non-zero angles, the tendency of the focusing mechanism to form a dominant viscous finger along the top boundary of the reservoir is reinforced by the emerging gravity tongue, resulting in early breakthrough. The left-propagating fronts, on the other hand, are characterized by vigorous viscous and/or gravitational fingering, which leads to the disintegration of the dominant finger along the bottom boundary.

rotation due to gravity, so that the front is oriented nearly in the vertical direction. As a result, there is a sufficient velocity component normal to the interface to produce strong viscous fingering. Note, however, that the topmost finger, adjacent to the upper reservoir boundary, is already more fully developed than the others and evolves into a gravity tongue. For long times, the effect of the non-uniform potential velocity field decreases, and the front is dominated by gravitational rotation for $\alpha = 15°$.

For $\alpha = 30°$ and 60°, the left-propagating fronts exhibit vigorous fingering as well. A comparison with the $G = 0$ counterparts in figure 10 demonstrates that this fingering is mostly driven by buoyancy forces. In these flows, the rotation of the left-propagating fronts by gravity does not occur rapidly enough, and the tangential velocity difference across the fronts is not sufficiently strong to suppress gravity-driven fingering. Eventually, the upward gravitational fingering results in the disintegration of the single viscous finger that had formed along the bottom boundary for $G = 0$. The rotational field associated with the left-propagating front indicates a weak anticlockwise vortex, which delays the propagation of the lower section of this front.

Increasing G to 1 intensifies the gravitational mechanisms and thus shifts some of the above balances. In particular, for $\alpha = 15°$ the left-propagating front now rotates into a stable position more rapidly, so that viscously driven fingering is suppressed: see figure 12. The same effect is observed for $\alpha = 30°$ between $G = 1$ and 2 (not shown).

The above simulation results demonstrate that for variable viscosity and density displacements the two fronts formed by an inclined injection well evolve very

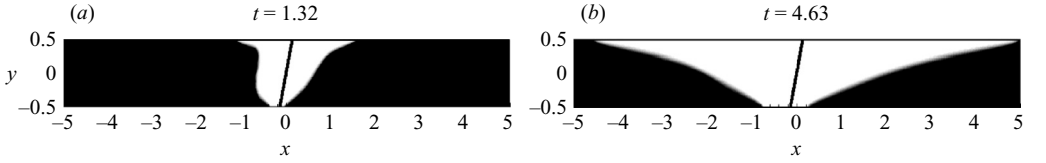

FIGURE 12. Early and late time displacement front for $R = 1$, $G = 1$, $Pe = 2000$ and $\alpha = 15°$. The stronger influence of gravity, as compared to the flow shown in figure 11, rapidly rotates the left-propagating front into a gravitationally stable position, thereby suppressing fingering.

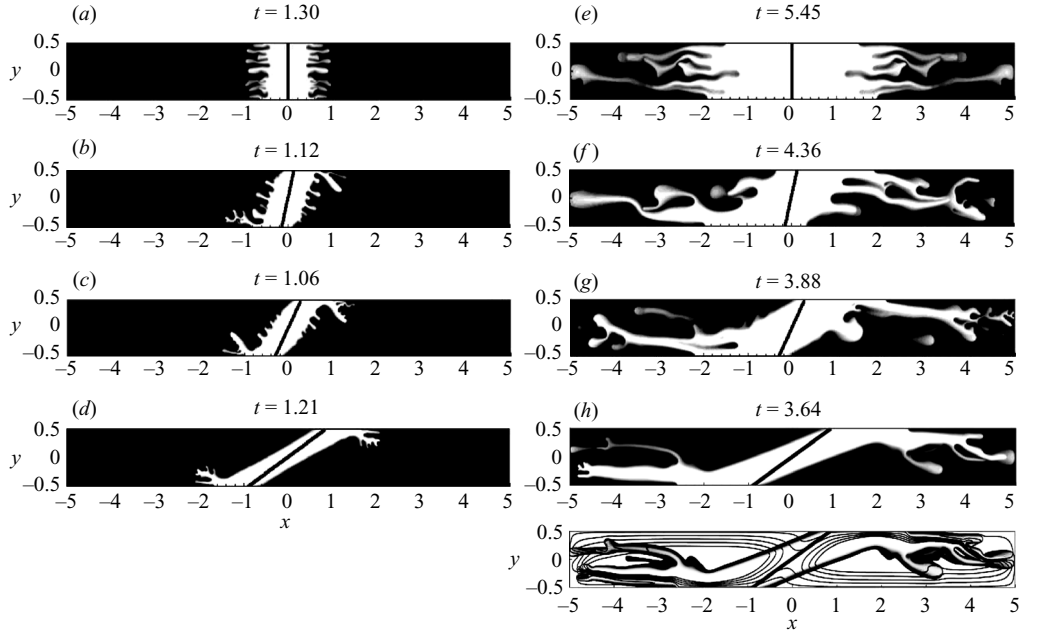

FIGURE 13. Displacement fronts for $R = 3$, $G = 0$, $Pe = 2000$ and $\alpha = 0°$, $15°$, $30°$ and $60°$, respectively. Similarly to lower mobility ratios, a single dominant finger quickly forms for each inclined front. However, in contrast to lower mobility ratio displacements, this dominant finger separates from the reservoir boundary and propagates towards the reservoir centreline, while undergoing repeated splitting events.

differently. For one front, the effects of gravity tongue formation and 'focused fingering' reinforce each other, so that a single dominant finger evolves which results in early breakthrough. The other front is characterized by a competition of these two effects, which leads to the disintegration of the dominant finger via viscous and gravitational instability.

4.3. *Flows dominated by viscosity differences,* $R = 3$

For a larger unfavourable viscosity difference of $R = 3$ and $G = 0$, some of the features seen earlier for $R = 1$ persist: see figure 13. The focusing of the fingering instability by the non-uniformities of the potential flow field is clearly visible, and it leads to the formation of a single dominant finger for each inclined front. Notice, in the bottom frame of the right column, that the rotational flow field has the form of two strong clockwise vortices, which accelerate the dominant fingers. For $\alpha = 60°$, much of the two fronts remains completely stable. However, at the higher

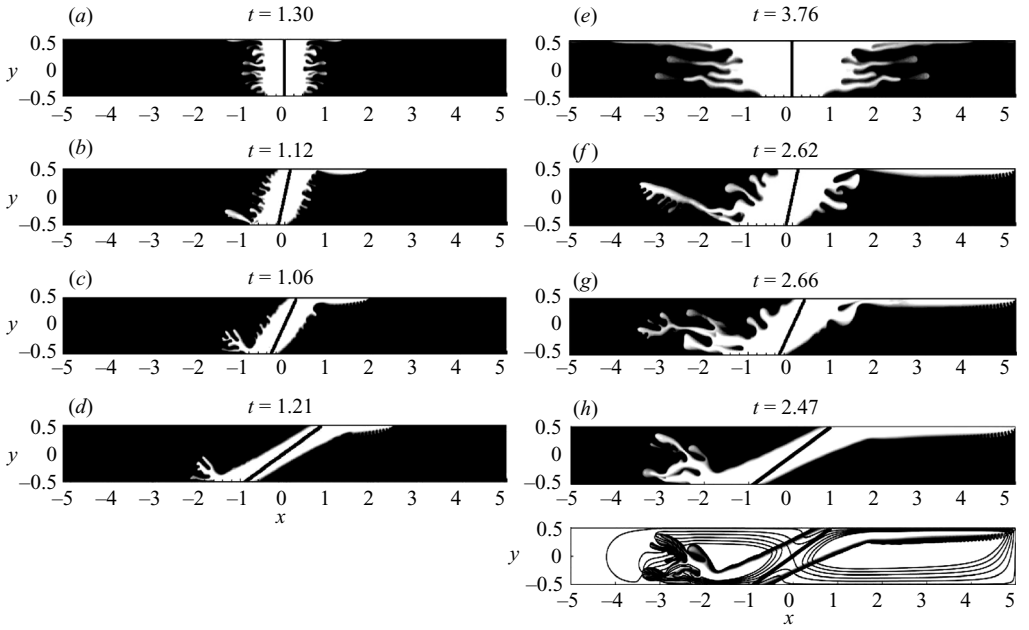

FIGURE 14. Displacement fronts for $R = 3$, $G = 0.5$, $Pe = 2000$ and $\alpha = 0°$, 15°, 30° and 60°, respectively. Along the right-propagating front, flow focusing and gravity tongue formation reinforce each other, whereas for the left-propagating front, they favour opposite trajectories for the injected fluid.

mobility ratio of $R = 3$ the dominant fingers do not remain attached to the reservoir boundaries, as had been the case for $R = 1$. Instead, they separate from the boundary and subsequently propagate towards the centreline of the reservoir. In this process, they give rise to strongly nonlinear dynamics including repeated shielding, splitting and merging events, similar to earlier findings for vertical injection wells (Tan & Homsy 1988; Tchelepi 1994; Ruith & Meiburg 2000; and others). Consequently, the fronts break through much earlier for $R = 3$, as compared to $R = 1$.

In the presence of a density contrast, $G > 0$, and for $\alpha > 0$, the focusing mechanism for generating a single dominant finger interacts with the tendency towards forming a gravity tongue: see figure 14. With regard to the right-propagating front, these two mechanisms reinforce each other, so that a dominant finger/gravity tongue propagates underneath the upper reservoir boundary. Note that for $\alpha = 15°$ and 30° a few secondary fingers initially emerge, whereas for $\alpha = 60°$ the front is completely stable below the gravity tongue. This is consistent with the findings for vertical source scenarios by Tchelepi (1994) and Ruith & Meiburg (2000). Interestingly, the gravity tongue can take a dendritic shape, with evenly spaced small branches forming in the downward direction. This feature will be discussed in more detail below.

For the left-propagating front, the focusing mechanism and the gravity tongue formation favour opposite tendencies: While the focusing mechanism generates a finger of the lighter, injected fluid at the lower boundary, gravity acts to collect the lighter fluid near the upper boundary. As a result, the dominant finger of lighter fluid that initially forms at the bottom soon separates from the lower boundary, splits repeatedly, and propagates towards the upper boundary. In this fashion, it bypasses

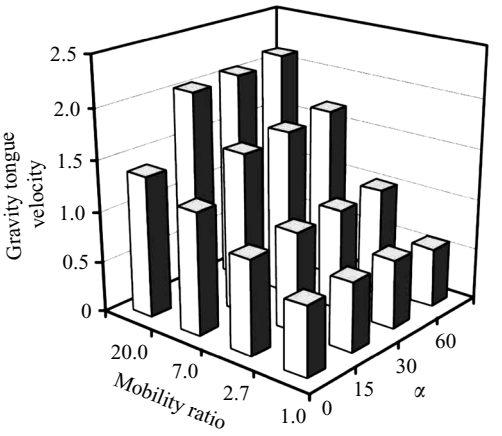

FIGURE 15. Quasi-steady propagation velocity of the gravity tongue for $G = 0.5$ and $Pe = 2000$, as a function of the viscosity ratio and the well inclination angle. The gravity tongue velocity is seen to depend strongly on the viscosity ratio, but it is nearly independent of the well inclination angle, for angles of 15° or larger.

and traps a substantial amount of the heavier fluid behind itself, thereby reducing the sweep efficiency.

Figure 15 presents a quantitative summary of the observed quasi-steady gravity tongue propagation velocities, as a function of the well inclination angle and the viscosity ratio. As expected, a larger viscosity ratio results in higher propagation velocities. Interestingly, the well angle has a much smaller effect: as long as the well is not aligned in the vertical direction, the magnitude of the well inclination affects the gravity tongue propagation velocity by no more than roughly 10 %.

4.4. *Dendritic fingering*

For high mobility ratios and $\alpha > 0$, several of our simulations exhibit dendritic fingering, in the sense of repeated, short-wavelength branching events of a main finger which itself largely stays intact. The ensuing fingering patterns are similar to earlier observations for immiscible flows (e.g. Couder *et al.* 1986*a*, *b*; Maxworthy 1986; Kopf-Sill & Homsy 1987; Meiburg & Homsy 1988). By analysing a large number of simulation results, we found that before such dendritic branching can occur, the main finger has to propagate far ahead of its neighbouring competitors, so that it is largely unconfined. Hence dendritic fingering is observed mostly for the dominant fingers that form as a result of the focusing mechanism, or for gravity tongues. All other fingers are more likely to exhibit the traditional tip splitting familiar from vertically oriented sources. An example of a dominant finger giving rise to dendritic branching is shown in figure 16. This type of dendritic branching usually occurs on the downstream side of a diagonally propagating dominant finger, where the interface is viscously unstable.

Even more dramatic can be the evolution of dendritic gravity tongues (see figures 14*b*, *f*, 14*c*, *g* and 14*d*, *h*). Here the side branches originate near the tip of the tongue, and subsequently propagate a finite distance downward. These dendritic side fingers do not move with the advancing tip of the gravity tongue. Rather, after being initiated by the passing tip of the gravity tongue, they remain at a constant streamwise location as they propagate downward. Note that these fingers form on the underside of the gravity tongue, which according to the traditional stability criteria should

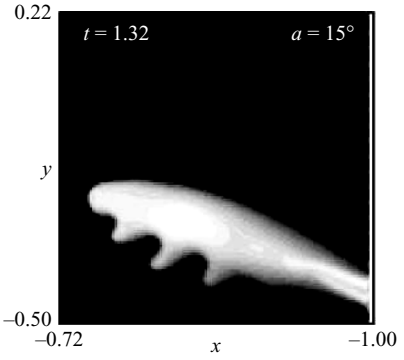

FIGURE 16. An example of dendritic branching on an unconfined dominant finger for $R = 3$, $G = 0.5$, $Pe = 2000$ and $\alpha = 15°$. The branching occurs on the downstream side, where the interface is viscously unstable.

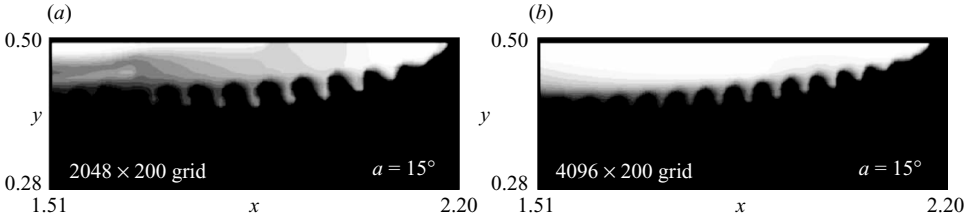

FIGURE 17. Comparison of a dendritically evolving gravity tongue for a coarse (2048×200) and a fine (4096×200) grid. The flow parameters are $R = 3$, $G = 0.5$, $Pe = 4000$ and $\alpha = 15°$. (*a*) A region of 140×44 grid points; (*b*) the same region discretized into 280×44 grid points. While the wavelength of the side branches depends weakly on the resolution, their overall properties remain unchanged.

be stable. Along this interface, the normal velocity is quite small, the density stratification is stabilizing, and there is a substantial tangential velocity difference, which should be stabilizing as well. Hence it is likely that the local dynamics at the tip of the gravity tongue plays a crucial role in the growth of the dendritic branches. Our simulations show that the tendency to form a dendritic gravity tongue is sensitive to the value of G. On one hand, a density difference between injected and displaced fluid is necessary to form the gravity tongue in the first place. On the other hand, if G is too large, it will suppress the downward growth of fingers of the lighter fluid into the heavier fluid. While we have not conducted an exhaustive study of the parameter range where dendritic gravity tongues appear, we have observed them for $R = 3$, $0.25 < G \leqslant 0.5$ and $15° \leqslant \alpha \leqslant 60°$.

Since the dendritic branches frequently represented the smallest features in our flow fields, we conducted additional, finer-resolution simulations to ensure that these structures were properly resolved. A typical comparison is shown in figure 17 for $\alpha = 15°$. The nature of the dendritic fingering is seen to remain unchanged as the resolution is doubled, although the streamwise wavelength is about 10–20% shorter for the finer grid. Most likely this reflects a weak influence of numerical diffusion. Note that this example is for a larger value of $Pe = 4000$, whereas all of the examples discussed above are for $Pe = 2000$, where the resolution requirements are lower.

5. Summary and conclusions

The present investigation provides insight into the mechanisms that dominate variable viscosity and density, miscible displacements generated by inclined injection sources. The numerical simulation results discussed above reveal significant differences compared to vertical injection wells, which strongly influence breakthrough times and recovery rates.

Preliminary simulations of constant density and viscosity displacements, for which the velocity field is potential in nature, demonstrate the existence of pronounced non-uniformities in the flow, due to the interaction of the inclined well with the upper and lower reservoir boundaries. Specifically, we observe the formation of stagnation points along the reservoir boundaries, and localized areas of increased flow velocities in the interior of the flow field, close to the boundaries. Even in the absence of viscosity and density contrasts, these regions of non-uniform flow strongly deform the interface during the initial displacement stages. When a viscosity difference is present, a focusing of the fingering instability results which leads to the formation of a dominant finger in the region of fastest potential flow. Its rapid growth leads to a much earlier breakthrough of the front than for vertical injection wells, thus reducing the efficiency of the displacement process. Hence any strategy for optimizing recovery rates for a given reservoir geometry should attempt to configure well in such a way that its interaction with the reservoir boundaries produces minimal potential flow non-uniformities.

In the presence of a density difference, interesting interactions and competitions between the dominant finger and the emerging gravity tongue are observed. Along one front, the dominant finger reinforces the gravity tongue, thereby accelerating it and further reducing its breakthrough time. For the other front, the dominant finger forms along the opposite boundary from where the gravity tongue would evolve. In this case, gravitational fingering in the direction normal to the dominant finger propagation usually leads to the rapid disintegration of this dominant finger. Hence, the two fronts emerging from the inclined injection well for variable density and viscosity displacements usually evolve very differently from each other. An important parameter is the ratio of the time scales governing the gravitational rotation of the interface and the growth of fingers.

For inclined injection wells and sufficiently large mobility ratios, dendritic fingering instabilities appear on the flanks of the dominant finger or, even more pronounced, along the exposed side of the gravity tongue. This happens when the dominant finger or gravity tongue is unconfined by any competing fingers. The formation of dendritic side branches on the gravity tongue is sensitive to the gravitational parameter. On one hand, gravitational forces are necessary to create the gravity tongue in the first place. On the other hand, if the density difference becomes too large, gravity will suppress the growth of the dendritic side branches, since they occur along the gravitationally stable side of the gravity tongue. In either case, the evolution of dendritic growth appears to require that the gravity tongue propagate significantly faster than its vertical injection well counterpart. Since the dendritic branches appear along the side of the gravity tongue that should be stable according to the traditional criteria, the tip region likely plays a crucial role in their formation. Efforts to unravel the underlying mechanisms behind this role of the tip are currently underway.

A further promising line of research could address the formulation of strategies for optimizing certain displacement properties. Depending on the particular application under consideration, one may want to delay or accelerate breakthrough, promote or

suppress mixing, or achieve various other flow properties. Towards this end, it would be interesting to explore if certain well angles result in optimal behaviour.

Thanks are due to Chevron Corporation and Occidental Petroleum Corporation for their support of this research. Acknowledgement is also made to the Donors of the American Chemical Society Petroleum Research Fund for partial support of this research through grant ACS PRF# 45175-AC9.

REFERENCES

Bacri, J. C., Rakotomalala, N., Salin, D. & Woumeni, R. 1992 Miscible viscous fingering: Experiments versus continuum approach. *Phys. Fluids* A **4**, 1611.

Bacri, J. C., Salin, D. & Woumeni, R. 1991 Three-dimensional miscible viscous fingering in porous media. *Phys. Rev. Lett.* **67**, 2005.

Bilhartz, H. L., Charlson, G. S., Stalkup, F. I. & Miller, C. C. 1978 A method of projecting full-scale performance of CO_2 flooding in the Willard Unit. *SPE AIME* **5**, 149.

Blackwell, R. J., Rayne, J. R. & Terry, W. M. 1959 Factors influencing the efficiency of miscible displacement. *Pet. Trans. AIME* **216**, 1.

Camhi, E., Meiburg, E. & Ruith, M. 2000 Miscible rectilinear displacements with gravity override. Part 2. Heterogeneous porous media. *J. Fluid Mech.* **420**, 259.

Canuto, C., Hussaini, M. Y., Quarteroni, A. & Zang, T. A. 1988 *Spectral Methods in Fluid Dynamics*. Springer.

Chen, C.-Y. & Meiburg, E. 1996 Miscible displacements in capillary tubes. Part 2. Numerical simulations. *J. Fluid Mech.* **326**, 57.

Chen, C.-Y. & Meiburg, E. 1998*a* Miscible porous media displacements in the quarter five-spot configuration. Part 1. The homogeneous case. *J. Fluid Mech.* **371**, 233.

Chen, C.-Y. & Meiburg, E. 1998*b* Miscible porous media displacements in the quarter five-spot configuration. Part 2. Effect of heterogeneities. *J. Fluid Mech.* **371**, 269.

Chouke, R., van Meurs, P. & vander Poel, C. 1959 The instability of slow, immiscible, viscous liquid–liquid displacements in permeable media. *Trans. AIME* **216**, 188.

Christie, M. A. 1989 High-resolution simulation of unstable flows in porous media. *SPE Res. Engng* **4**, 297.

Christie, M. A. & Bond, D. J. 1986 Detailed simulation of unstable processes in miscible flooding. *SPE/DOE Paper* 14896.

Christie, M. A., Jones, A. D. W. & Muggeridge, A. H. 1990 Comparison between laboratory experiments and detailed simulations of unstable miscible displacement influenced by gravity. In *North Sea Oil and Gas Reservoirs II*. Graham and Trotman .

Coskuner, G. & Bentsen, R. G. 1990 An extended theory to predict the onset of viscous instabilities for miscible displacements in porous media. *Trans. Por. Med.* **5**, 473.

Couder, Y., Cardoso, O., Dupuy, D., Tavernier, P. & Thom, W. 1986*a* Dendritic growth in the Saffman–Taylor experiment. *Europhys. Lett.* **2**, 437.

Couder, Y., Gerard, N. & Rabaud, M. 1986*b* Narrow fingers in the Saffman–Taylor instability. *Phys. Rev.* A **34**, 5175.

De Josselin De Jong, G. 1960 Singularity distributions for the analysis of multiple-fluid flow through porous media. *J. Geophys. Res.* **65**, 3739.

De Wit, A. & Homsy, G. M. 1999 Nonlinear interactions of chemical reactions and viscous fingering in porous media. *Phys. Fluids* **11**, 949.

Gardner, J. W. & Ypma, J. G. J. 1984 An investigation of phase behavior/macroscopic-bypassing interaction in CO_2 flooding. *SPE J.* **24**, 508.

Heller, J. P. 1963 The interpretation of model experiments for the displacement of fluids through porous media. *AIChE J.* **9**, 452.

Hickernell, J. F. & Yortsos, Y. C. 1986 Linear stability of miscible displacement processes in porous media in the absence of dispersion. *Stud. Appl. Math.* **74**, 93.

Hill, S. 1952 Channelling in packed columns. *Chem. Engng Sci.* **1**, 247.

Homsy, G. M. 1987 Viscous Fingering in Porous Media. *Ann. Rev. Fluid Mech.* **19**, 271.

Howard, G. C. & Fast, C. R. 1970 *Hydraulic Fracturing, Monograph 2*. SPE, Richardson, TX.

Kopf-Sill, A. R. & Homsy, G. M. 1987 Narrow fingers in a Hele–Shaw cell. *Phys. Fluids* **30**, 2607.

Lamb, H. 1932 *Hydrodynamics*. Cambridge University Press.

Lele, S. 1992 Compact finite difference schemes with spectral-like resolution. *J. Comput. Phys.* **103**, 16.

Manickam, O. & Homsy, G. M. 1993 Stability of miscible displacements in porous media with nonmonotonic viscosity profiles. *Phys. Fluids* **5**, 1356.

Manickam, O. & Homsy, G. M. 1994 Simulation of viscous fingering in miscible displacements with nonmonotonic viscosity profiles. *Phys. Fluids* **6**, 95.

Manickam, O. & Homsy, G. M. 1995 Fingering instabilities in vertical miscible displacement flows in porous media. *J. Fluid Mech.* **288**, 75.

Maxworthy, T. 1986 Bubble formation, motion and interaction in a Hele–Shaw cell. *J. Fluid Mech.* **173**, 95.

Meiburg, E. & Homsy, G. M. 1988 Nonlinear unstable viscous fingers in Hele–Shaw flows. II. Numerical simulation. *Phys. Fluids* **31**, 429.

Pankiewitz, C. & Meiburg, E. 1999 Miscible porous media displacements in the quarter five-spot configuration. Part 3. Nonmonotonic viscosity profiles. *J. Fluid Mech.* **388**, 171.

Peaceman, D. W. & Rachford, H. H. 1955 The numerical solution of parabolic and elliptic differential equations. *SIAM J.* **3**, 28.

Peaceman, D. W. & Rachford, H. H. 1962 Numerical calculation of multi-dimensional miscible displacement. *Soc. Pet. Engng. J.* **24**, 327.

Perkins, T. K. & Johnston, O. C. 1963 A review of diffusion and dispersion in porous media. *SPE J.* **3**, 195.

Petitjeans, P., Chen, C.-Y., Meiburg, E. & Maxworthy, T. 1999 Miscible quarter five-spot displacements in a Hele–Shaw cell and the role of flow-induced dispersion. *Phys. Fluids* **11**, 1705.

Petitjeans, P. & Maxworthy, T. 1996 Miscible displacements in capillary tubes. Part 1. Experiments. *J. Fluid Mech.* **326**, 37.

van der Poel, C. 1962 *SPE J. Trans. AIME* **225**, 317.

Riaz, A. & Meiburg, E. 2003*a* Radial source flows in porous media: Linear stability analysis of axial and helical perturbations in miscible displacements. *Phys. Fluids* **19**, 938.

Riaz, A. & Meiburg, E. 2003*b* Three-dimensional miscible displacement simulations in homogene ous porous media with gravity override. *J. Fluid Mech.* **494**, 95.

Riaz, A. & Meiburg, E. 2004 Vorticity interaction mechanisms in variable viscosity, heterogeneous miscible displacements with and without density contrast. *J. Fluid Mech.* **517**, 1.

Riaz, A., Pankiewitz, C. & Meiburg, E. 2004 Linear stability of radial displacements in porous media: Influence of velocity-induced dispersion and concentration-dependent diffusion. *Phys. Fluids* **16**, 3592.

Rogerson, A. & Meiburg, E. 1993*a* Numerical simulation of miscible displacement processes in porous media flows under gravity. *Phys. Fluids* A **5**, 2644.

Rogerson, A. & Meiburg, E. 1993*b* Shear stabilization of miscible displacement processes in porous media. *Phys. Fluids* A **5**, 1344.

Ruith, M. & Meiburg, E. 2000 Miscible rectilinear displacements with gravity override. Part 1. Homogeneous porous medium. *J. Fluid Mech.* **420**, 225.

Saffman, P. G. & Taylor, G. 1958 The penetration of a fluid into a porous medium or Hele–Shaw cell containing a more viscous fluid. *Proc. R. Soc. Lond.* A **245**, 312.

Stalkup, F. I. 1983 *Miscible Displacement*. SPE, Richardson, TX.

Taber, J. J. & Seright, R. S. 1992 Horizontal injection and production wells for EOR or waterflooding. *SPE Paper* 23952.

Tan, C. T. & Homsy, G. M. 1986 Stability of miscible displacements in porous media: Rectilinear flow. *Phys. Fluids* **29**, 3549.

Tan, C. T. & Homsy, G. M. 1987 Stability of miscible displacements in porous media: Radial source flow. *Phys. Fluids* **30**, 1239.

Tan, C. T. & Homsy, G. M. 1988 Simulation of nonlinear viscous fingering in miscible displacement. *Phys. Fluids* **31**, 1330.

Tan, C. T. & Homsy, G. M. 1992 Viscous fingering with permeability heterogeneity. *Phys. Fluids* A **4**, 1099.

Taylor, G. 1953 Dispersion of soluble matter in solvent flowing slowly through a tube. *Proc. R. Soc. Lond.* A, **219**, 186.

Tchelepi, H. A. 1994 Viscous fingering, gravity segregation and permeability heterogeneity in two-dimensional and three dimensional flows. PhD thesis, Department of Petroleum Engineering, Stanford University.

Tryggvason, G. & Aref, H. 1983 Numerical experiments on Hele Shaw flow with a sharp interface. *J. Fluid Mech.* **136**, 1.

Upchurch, E. R. 2005 The effects of injection source inclination, stratified permeability heterogeneity and permeability anisotropy on the miscible flooding of porous media. PhD thesis, University of Southern California, Los Angeles, CA.

Wright, C. A. & Conant, R. A. 1995 Hydraulic fracture reorientation in primary and secondary recovery from low-permeability reservoirs. *SPE Paper* 30484.

Yang, Z. M. & Yortsos, Y. C. 1998 Effect of no-flow boundaries on viscous fingering in porous media of large aspect ratio. *SPE J.* **3**, 285.

Yortsos, Y. C. 1990 Instabilities in displacement processes in porous media. *J. Phys. Condens. Matter* **2**.

Yortsos, Y. C. & Zeybek, M. 1988 Dispersion driven instability in miscible displacement in porous media. *Phys. Fluids.* **31**, 3511.

Zimmerman, W. B. & Homsy, G. M. 1991 Nonlinear viscous fingering in miscible displacement with anisotropic dispersion. *Phys. Fluids* A **3**, 1859.

Zimmerman, W. B. & Homsy, G. M. 1992*a* Three-dimensional viscous fingering: A numerical study. *Phys. Fluids* A **4**, 1901.

Zimmerman, W. B. & Homsy, G. M. 1992*b* Viscous fingering in miscible displacements: Unification of effects of viscosity contrast, anisotropic dispersion, and velocity dependence of dispersion on nonlinear propagation. *Phys. Fluids* A **4**, 2348.